This is a preprint, the final version is subject to change, of the American Mineralogist (MSA)
Cite as Authors (Year) Title. American Mineralogist, in press.
DOI: https://doi.org/10.2138/am-2020-7324

Revision 1

Regular article

Raman spectroscopic studies of O–H stretching vibration in Mn-rich apatites: a structural approach

Raman spectroscopic studies of O–H stretching vibration in Mn-rich apatites

ADAM PIECZKA[1]*, BOŻENA GOŁĘBIOWSKA[1], PIOTR JELEŃ[2], MACIEJ SITARZ[2] AND ADAM SZUSZKIEWICZ[3]

[1] Department of Mineralogy, Petrography and Geochemistry, AGH University of Science and Technology, Mickiewicza 30, 30-059 Kraków, Poland; goleb@agh.edu.pl

[2] Faculty of Materials Science and Ceramics, AGH University of Science and Technology, Mickiewicza 30, 30-059 Kraków, Poland; pjelen@agh.edu.pl, msitarz@agh.edu.pl

[3] University of Wrocław, Institute of Geological Sciences, 50-204 Wrocław, pl. M. Borna 9, Poland; adam.szuszkiewicz@uwr.edu.pl

**corresponding author*: pieczka@agh.edu.pl

Abstract

The O–H stretching vibration mode in crystals of (Mn,Cl)-rich and F-poor minerals of the apatite-supergroup has been studied by micro-Raman spectroscopy. The main purpose was to check if such an analysis can provide a quick and simple method to assess the distribution of Ca

and Mn together with traces of Fe + Mg (=Mn*) on nonequivalent cationic sites in the apatite structure, especially in small and strongly heterogeneous crystals directly in thin sections. The O–H stretching vibration mode can then be treated as a useful structural probe giving information on the M2 occupants bonded to ^{X}OH. Pieczkaite, with the empirical formula $(Mn_{4.49}Fe_{0.47}Ca_{0.05}Mg_{0.01})_{\Sigma 5.01}P_{2.99}O_{12}[Cl_{0.83}(OH)_{0.17}]$, displays the O–H stretching mode centered at ~3380 cm^{-1}, which shows that the complete replacement of Ca by Mn* at the M2 site is connected with a shift of the O–H stretching band ~192 cm^{-1} towards lower wavenumbers in relation to the O–H Raman band position reported for hydroxylapatite. The value is high enough to be an indicator of the ^{M2}Mn*…OH content in any sample of Mn-enriched apatite. Studies of the fine structure of the band disclosed its dependence on (*i*) the local combinations of Ca and Mn* forming triplets of M2 cations bonded to the X anion, (*ii*) the presence of OH + Cl at the two half-occupied X sites that form chemical bonds with the M2 cations varying in strength and length, (*iii*) the spatial geometry of the X–M2 bonds and polarizability of the monovalent X anion by varying cations in the M2M2M2 triplets. The deconvolution of the band into maximum eight component bands with constant Raman shifts opens the possibility of evaluating the averaged M2M2M2 triplet bonded to oxygen of the ^{X}OH group. If the OH/(OH+Cl) fraction is known, the amounts of Ca and Mn* bonded to ^{X}OH can also be estimated. Application of the method to the holotype parafiniukite showed a slightly different distribution of Ca in M2M2M2 triplets than had been assumed from single-crystal X-ray diffraction. However, it corroborates suggestions that in the apatite structure there may be a preference for ^{M2}Ca to be bonded to ^{X}OH, and ^{M2}Mn* to ^{X}Cl. Our results show that the proposed method can be used as an independent tool in structural studies of Mn-rich minerals of the apatite-supergroup, providing results complementary to single-crystal X-ray diffraction. This method can easily be adjusted to modern apatite-type nanomaterials synthesized for biomedical and various industrial applications.

Keywords: Mn-bearing minerals of the apatite supergroup, Raman spectroscopy, O–H stretching vibration, pieczkaite, parafiniukite.

INTRODUCTION

Pieczkaite, ideally $Mn_2Mn_3(PO_4)_3Cl$, and parafiniukite, ideally $Ca_2Mn_3(PO_4)_3Cl$, are two (Mn,Cl)-dominant apatite-supergroup minerals described recently from two highly Mn-Fe fractionated granitic pegmatites of the Li–Cs–Ta (LCT) petrogenetic family at Cross Lake, Manitoba, Canada, and at Szklary, Lower Silesia, Poland (Tait et al. 2015; Pieczka et al. 2018). Both minerals were also recognized in phosphate nodules of an LCT-type pod within the hybrid NYF (Nb–Y–F) + LCT Julianna pegmatitic system at Piława Górna, Lower Silesia, Poland (Twardak and Pieczka 2018). In pieczkaite and parafiniukite F is commonly absent or occurs only in traces and the dominant monovalent anion is Cl. On the other hand, the OH group is usually an important minor constituent substituting for Cl. The structures of both minerals have been determined and spectroscopic measurements in the range of the O–H stretching vibration mode have confirmed the existence of Cl–OH solid solutions (Tait et al. 2015; Pieczka et al. 2018).

In studying phosphates of the apatite supergroup with compositions determined by the Mn↔Ca substitution, the Mn-Ca ordering between the two nonequivalent cation sites is of primary importance (e.g. Tait et al. 2015; Pieczka et al. 2018; Szuszkiewicz et al. 2018). Therefore, a quick and simple method providing such information even from small crystals directly in petrographic thin sections would be a very useful research tool. In this study we demonstrate that Raman micro-spectroscopy can be successfully employed for that purpose.

BACKGROUND INFORMATION ON MN-BEARING APATITES

Pieczkaite and parafiniukite crystallize in hexagonal space-group symmetry $P6_3/m$ with unit-cell parameters a = 9.504(4) and 9.4900(6) Å, and c = 6.347(3) and 6.4777(5) Å, respectively (Tait et al. 2015; Pieczka et al. 2018). Accepting the generic formula of the apatite supergroup $^{IX}M1_2{}^{VII–}{}^{IX}M2_3(TO_4)_3X$ (Z=2), the M sites can incorporate a wide range of cations such as Ca^{2+}, Pb^{2+}, Ba^{2+}, Sr^{2+}, Mn^{2+}, Na^{+}, Ln^{3+} (lanthanides), Y^{3+}, Bi^{3+}; while T = P^{5+}, As^{5+}, V^{5+}, Si^{4+}, S^{6+}, B^{3+}; and X = $F^{–}$, $OH^{–}$, $Cl^{–}$, and $O^{2–}$ (Pasero et al. 2010). Both minerals have the Mn-dominant M2 site and Cl-dominant X site. The M1 site is occupied predominantly by Mn in pieczkaite and by Ca in parafiniukite, giving the ideal formulas of $^{M1}Mn_2{}^{M2}Mn_3(PO_4)_3Cl$ and $^{M1}Ca_2{}^{M2}Mn_3(PO_4)_3Cl$, respectively. As in chlorapatite, $Ca_5(PO_4)_3Cl$, and hydroxylapatite, $Ca_5(PO_4)_3OH$, in parafiniukite and pieczkaite each M2 cation coordinates two half-occupied X sites displaced off the mirror plane at z = 1/4. As a result, the X anion surrounded by six M2 cations is bonded formally to three M2 cations at distances in the range of 2.23–2.80 Å (Tait et al. 2015; Pieczka et al. 2018). In fluorapatite, $Ca_5(PO_4)_3F$, one X site located at the mirror plate is fully occupied by F.

For the apatite-supergroup phosphates with unlimited degrees of Mn↔Ca and F↔Cl↔OH substitutions, the exact classification must be based on the distribution of Mn and Ca between the nonequivalent M1 and M2 sites and on the dominant X-site anion. Assuming that the Mn-Ca ordering and X-site occupancy are independent of each other, the following structural variants can exist:

- with Mn ≤ 1.0 atom per formula unit (apfu), only fluor-, hydroxyl- or chlorapatite are possible;
- with 1 < Mn ≤ 1.5 apfu, the minerals can still be fluor-, hydroxyl- or chlorapatite but, if Mn is dominantly ordered at the M1 site, they may also represent three possible new species corresponding to the formula $Mn_2Ca_3(PO_4)_3X$;

- with $1.5 < Mn \leq 2.5$, the minerals can represent structurally disordered fluor-, hydroxyl- or chlorapatites (albeit extremely Mn-enriched), but, with a sufficient degree of structural order, also $Mn_2Ca_3(PO_4)_3X$ or even $Ca_2Mn_3(PO_4)_3X$ species; the latter at $Cl > 0.5$ apfu would correspond to parafiniukite;
- with $2.5 < Mn \leq 3.5$ apfu, $Mn_2Ca_3(PO_4)_3X$, $Ca_2Mn_3(PO_4)_3X$ and pieczkaite-type species $Mn_2Mn_3(PO_4)_3X$ (pieczkaite for $Cl > 0.5$ apfu) are possible;
- with $3.5 < Mn \leq 4$ apfu, only species with $Ca_2Mn_3(PO_4)_3X$ or $Mn_2Mn_3(PO_4)_3X$ stoichiometry exist;
- with $Mn > 4$ apfu, the minerals represent one of the pieczkaite-type species $Mn_2Mn_3(PO_4)_3X$ (pieczkaite for $Cl > 0.5$ apfu).

The scheme can be further complicated if the Mn-Ca ordering is dependent on the X-site occupancy. For instance, it has been observed for pieczkaite, parafiniukite and Mn-rich fluorapatite that if Cl is present in significant quantity at the X site, the M2-X distance becomes shortened in relation to that in chlorapatite, indicating a preference for a smaller cation, i.e. Mn, to enter the M2 position; the M1 site is favored by Mn if the X site is dominated by F (Suitch et al. 1985; Hughes et al. 2004, 2016; Tait et al. 2011, 2015; Pieczka et al. 2018). It is, however, not clear if a fully Mn-Ca ordered structure can be achieved with X sites populated by a significant share of all the F, Cl and OH anions.

All being considered, an exact classification of Mn-rich members of the apatite supergroup is not straightforward and almost always requires structural analysis to determine the distribution of Mn and Ca between the cationic sites as it was already pointed out by Szuszkiewicz et al. (2018). Although single-crystal X-ray diffraction is available in many laboratories, it requires extraction of a compositionally homogeneous crystal fragment commonly with sizes from a few tens to single micrometers, sometimes from a polycrystalline matrix. Therefore, the application of this

method is often problematic or even impossible, especially in the case of grains with sizes below 10–20 μm or if crystals have highly heterogeneous chemical compositions. As a result, structural information is usually lacking for such material. Minerals of the parafiniukite-pieczkaite series are found as very small and often patchily-zoned grains, and sometimes as polycrystalline aggregates (Cross Lake, Piława Górna). Only in the Szklary pegmatite have exceptionally rare crystals of pieczkaite-parafiniukite compositions, reaching 200 μm in size, been found. Therefore, micro-Raman spectroscopy seems to be the most suitable method for crystal chemical and structural studies of such minerals. This technique does not require sample preparation, is non-destructive and effectively provides a structural fingerprint of a specific species. Additionally, it operates with micrometer-scale spatial resolution, usually ~1 μm^2.

MATERIAL AND METHODS

The research material for the quantitative chemical and spectroscopic studies comprised crystals of the (Mn,Cl)-rich apatite-supergroup minerals with a stoichiometry corresponding to the pieczkaite-parafiniukite solid solution, $Mn_2Mn_3(PO_4)_3Cl$–$Ca_2Mn_3(PO_4)_3Cl$, from the granitic pegmatite at Szklary, Lower Silesia, Poland. They typically occur as relic grains, up to 200 μm large, intergrown either in beusite partly altered into Mn-oxides and smectites or in Mn-bearing fluorapatite. Rare single crystals included in muscovite are also observed. The compositional variation, microtextural relationships and possible origin of most of these crystals were studied by Szuszkiewicz et al. (2018) and Pieczka et al. (2018). These contributions also give detailed information on the provenance and mode of occurrence of the samples. Here, we retain the original labeling of the pieczkaite-parafiniukite-bearing samples (Sz29, Sz31, Sz97 and Sz108). For the current study, all these samples were re-investigated with electron microprobe in order to locate crystals or parts of the crystals that are compositionally homogeneous and represent

different parts of the pieczkaite-parafiniukite solid solution. This re-examination revealed also the presence of 10–20 μm large crystals of nearly pure end-member pieczkaite in sample Sz29, overlooked in previous investigations (Fig. 1). Finally, six groups of crystals or crystal domains with distinct compositions were selected for the spectroscopic studies. The crystals labeled Sz29 represent pieczkaite, those from sample Sz31 are the holotypic parafiniukite, and the remaining samples used in this study, Sz97 and Sz108, are two compositionally heterogeneous (Mn,Cl)-rich apatites for which electron microprobe analyses and Raman spectra were collected in the Mn-richest and Mn-poorest domains (Sz97/2 and Sz97/6, and Sz108/6 and Sz108/9, respectively).

Electron probe microanalysis (EPMA)

Chemical analyses were carried out at the Inter-Institute Analytical Complex for Minerals and Synthetic Substances at the University of Warsaw, Poland, using a Cameca SX 100 electron microprobe operating in wavelength-dispersive (WDS) mode under the following conditions: accelerating voltage of 15 kV, beam current of 20 nA and beam diameter of 2 μm. Standards (element, emission line) were: fluorophlogopite (F, *K*α), $YbPO_4$ (P, *K*α), hematite (Fe, *K*α), rhodonite (Mn, *K*α), diopside (Mg, *K*α; Si, *K*α; Ca, *K*α), albite (Na, *K*α), tugtupite (Cl, *K*α), orthoclase (Al, *K*α; K, *K*α), celestine (Sr, *L*α), baryte (S, *K*α; Ba, *L*α), crocoite (Pb, *M*α), sphalerite (Zn, *K*α) and GaAs (As, *L*α). The following diffracting crystals were used: PC0 for F; TAP for Na, Mg, Al, Si and As; LPET for P, S, Cl, K, Ca, Sr and Pb; LLIF for Mn, Fe, Zn and Ba. Other elements such as Al, Si, S, K, Zn, Sr, As, Ba and Pb were below detection limits. The raw data were reduced with the PAP routine of Pouchou and Pichoir (1991) using CAMECA software for the electron microprobe. Direct H_2O determination was not performed due to the extremely small grain sizes of the available material; however, the occurrence of H_2O confirmed by Raman spectroscopy (Fig. 2) was calculated according to stoichiometry of the apatite-

supergroup minerals to obtain 1 (OH + F + Cl) apfu. The contents of atoms in the formulas were calculated to obtain 12 O + 1 (F,Cl,OH) apfu (Table 1).

Micro-Raman spectroscopy (RS)

Unpolarized Raman spectra were collected in back-scattered geometry at the Faculty of Materials Science and Ceramics, AGH UST, Cracow, Poland, with a Horiba Labram HR spectrometer integrated with an Olympus BX 41 confocal microscope. The system was calibrated using the 520.7 cm^{-1} Raman band of Si. The spectra were recorded in the range 50–4000 cm^{-1} using the 532 nm line of a solid-state Nd-YAG laser (10 mW) and 1800 gr/mm grating, on surfaces of randomly oriented crystals present in small fragments of the pegmatite mounted in epoxy resin. The same crystals were used for the EPMA studies. The Raman measurements were carried out by accumulation of two scans with precision ± 0.39 cm^{-1}, each with an acquisition time of 600 s at the microscope magnification 100×; the minimum lateral and depth resolution ~1 μm, and an estimated analytical spot size of ~1 μm.

The deconvolution of the O–H stretching mode was done in the range of 3300–3600 cm^{-1} applying the FITYK program for data processing and nonlinear curve fitting (Wojdyr 2010), after subtracting a linear background. To identify hidden bands, peak positions, full-widths at half maximum (FWHM), and integrated intensities were determined by fitting with Gaussian function shapes and application of the Levenberg-Marquardt fitting algorithm (Levenberg 1944; Marquardt 1963). The initial spectral position, height and FWHM of anticipated bands were matched in such a way as to minimize the difference between the empirical and theoretical spectrum designated as the sum of intensities of the anticipated bands, considering the fine structure of the spectra.

RESULTS AND DISCUSSION

The micro-Raman spectra of the (Mn,Cl)-rich apatites recorded in the Raman shift range of 50–4000 cm^{-1} are shown in Figure 2. The bands in the ranges ~930–1100, ~400–700, and below 300 cm^{-1} are related, respectively, to stretching and bending modes in the PO_4 groups, and deformations of the Ca and Mn polyhedra in the apatite structure. The band at ~3300–3600 cm^{-1}, which is the object of this research, is from stretching vibrations of O–H bond (Tait et al. 2015; Pieczka et al. 2018). The relative intensities of the O–H stretching vibration band are low, distinctly below 10 % of the most intense band. For compositionally homogeneous groups of crystals the spectral range of O–H stretching vibrations seems to be identical. However, the intensities of this band vary from crystal to crystal, probably due to various crystallographic orientations (Figure 3).

O–H stretching vibration range

Careful analysis of the spectral position of the band related to the O–H stretching mode in (Mn,Cl)-rich apatite-supergroup minerals reveals a very strong negative correlation of Raman shift values and the ^{M2}Mn content. The compositions of the analyzed minerals can be treated as solid solutions of hydroxylapatite, $^{M1}Ca_2{}^{M2}Ca_3(PO_4)_3OH$, and pieczkaite, $^{M1}Mn_2{}^{M2}Mn_3(PO_4)_3Cl$, with possible cation ordering between the M1 and M2 sites. Therefore, assuming proportional displacement of the band in relation to Mn/(Ca+Mn) atomic ratio, its approximate position in each spectrum can be determined from the relationship: $v = v_{\text{hydroxylapatite}} \cdot n + v_{\text{pieczkaite}} \cdot (1\text{-}n)$, where n is the molar content of hydroxylapatite in the solid solution and v denotes Raman shift. The IR / Raman spectrum of pure hydroxylapatite is well known and the O–H stretching vibration has been observed at 3572 cm^{-1} (Fowler 1974; Tsuda and Arends 1994; Rehman and Bonfield 1997; Zakharov et al. 2004), 3573 cm^{-1} (Penel et al. 2003) and 3576 cm^{-1} (Cuscó et al. 1998). However, before pieczkaite with a nearly ideal end-member composition was found, direct determination of the position of the ^{M2}Mn…O–H stretching band was impossible. The Raman

spectrum of pieczkaite Sz29, with the composition $(Mn_{4.49}Fe_{0.47}Ca_{0.05}Mg_{0.01})_{\Sigma 5.01}P_{2.99}O_{12}[Cl_{0.83}(OH)_{0.17}]$, shows the O–H stretching mode centered at ~3380 cm^{-1} (Figure 3). Thus, combining Mn^{2+} with subordinate Fe^{2+} and traces of Mg^{2+} (Mn* = Mn + Fe + Mg), the replacement of Ca by Mn* at the M2 site of the apatite structure is connected with the occurrence of the O–H stretching mode at lower Raman shift value by ~192 cm^{-1} compared to the O–H stretching mode reported in pure hydroxylapatite. This could denote that the replacement of Ca by Mn* at the M2 at an amount of 1 apfu decreases the position of the O–H stretching mode by ~64 cm^{-1}. The change of the Raman shift value is high enough to be an indicator of the ^{M2}Mn*…OH content in any sample of (Mn,OH)-enriched apatite. For the parafiniukite Sz31, the position of the band at ~3485 cm^{-1} (Pieczka et al. 2018) allows estimation of 1.36 ^{M2}Mn* apfu and 1.64 ^{M2}Ca apfu bonded to 1 OH(+F) group. In this specimen, OH + F occupy the X position in 52 % implying that only ~0.71 ^{M2}Mn* apfu is bonded to the X-site occupants other than Cl, and that the ^{M2}Ca content is ~0.85 apfu. Because the results of the X-ray structure refinement indicate that the M2-site is populated by 1.94 Mn* + 1.06 Ca (Pieczka et al. 2018), ^{X}Cl should be bonded to ~1.23 ^{M2}Mn* + 0.21 ^{M2}Ca apfu.

Fine structure of the O–H stretching band

The model discussed above explains well the occurrence of the O–H stretching mode at lower Raman shift values in the Raman and IR spectra of (Mn,Cl)-rich apatites when Ca is substituted by Mn*. However, it does not explain the noticeable asymmetry of the O–H Raman band related to the fine spectrum structure. Tait et al. (2015) suggested that the fine structure of the ^{X}OH band in pieczkaite results from local combinations of Ca and Mn forming triplets of M2 cations bonded to the X anion: OH-CaCaCa, OH-CaCaMn, OH-CaMnMn and OH-MnMnMn (in order of decreasing Raman shifts as coordinating ions of greater mass displace the associated OH absorption to lower wavenumbers). We adopt this idea to deconvolute the O–H stretching mode

in all the obtained spectra. Deconvolution was done with the positions of the component bands fixed at 3572, 3380, 3444 and 3508 cm^{-1}. The positions were designated as characteristic (1) for the triplet OH-CaCaCa on the basis of the O–H stretching mode in pure hydroxylapatite (Fowler 1974; Tsuda and Arends 1994; Rehman and Bonfield 1997; Zakharov et al. 2004); (2) for the triplet OH-Mn*Mn*Mn* by position of the main band in the spectrum of the pieczkaite Sz29; and (3) for the remaining two triplets OH-CaMn*Mn* and OH-CaCaMn*, respectively, calculated through the subtraction of 128 cm^{-1} and 64 cm^{-1} from the spectral position of OH-CaCaCa when two or one Ca atom in the triplet is replaced by Mn*. Results of the deconvolution presented in Figure 4 along with a plot of residuals show a relatively large unfitted portion of the spectrum for all the fitted spectra. On the other hand, the deconvolution with free peak positions of the intermediate component bands related to the OH-CaMn*Mn* and OH-CaCaMn* triplets significantly improve the fittings results (Fig. 5). This indicates that the nature of the O–H stretching mode in apatite-supergroup minerals is more complex, and it is impossible to explain its fine structure only by the occupancy of the M2 triplet bonded to ^{X}OH.

Is there any other factor that can affect the spectra? To answer this question, the substitution Cl↔OH at the X site in the pieczkaite–parafiniukite series will be briefly discussed. In the structure of pieczkaite, parafiniukite and hydroxylapatite forming an isomorphic group, the X site is subdivided into two subsites, X_a and X_b, placed slightly below and above the mirror plane at z = ¼ and surrounded by six M2 cations. Generally, the monovalent anion in all these minerals is shifted from the centre of the X–$(M2)_6$ octahedron towards the octahedron face, in contrast to the structure of chlorapatite, where it is closer to the center of this octahedron (Tait et al. 2015). Because the distance between the X_a and X_b subsites is too small, only one of them can be locally occupied by the monovalent X anion (so-called half-occupied X site). For instance, in holotypic pieczkaite, the anion, $Cl_{0.62}OH_{0.38}$, was observed as placed slightly off the mirror plane and

forming three bonds to M2 cations placed within the mirror with distances 2.477(2) Å (Tait et al. 2015). In holotypic parafiniukite, the monovalent anion, $Cl_{0.48}OH_{0.41}F_{0.11}$, is placed in a major portion (X_a = 0.78 apfu) within the mirror plane and, in a smaller portion (X_b = 0.24 apfu) slightly off the mirror plane. For this reason, it forms six bonds to M2 cations, of which three bonds are stronger (individual bond valence ~0.26 valence unit, *vu*), and the others are weaker (~0.08 *vu*), respectively with distances 2.431(2) Å and 2.466(4) Å (Pieczka et al. 2018). These data indicate that in the structure of the pieczkaite-parafiniukite solid solution, two general types of M2 triplets can be present: one with shorter OH–M2 and weaker O–H bonds, $(OH)_a$–M2M2M2, and the other with longer OH–M2 and stronger O–H bonds, $(OH)_b$–M2M2M2. The spatial geometry of the X–M2 bonds and polarizability of the monovalent X anion by action of the bonded M2 cations (with different mass and numbers of protons in their nuclei) may still be another local influence. In case of ^{X}OH groups, this influence would manifest itself through the fine structure of their O–H stretching mode.

To predict the spectral positions of the component bands related to the O–H stretching mode in the studied Raman spectra, we took into account four triplets of M2 cations, and two possible types of OH groups bonded with the triplets by stronger and weaker bonds. Together, they give eight possible arrangements (Table 2). Furthermore, we accept that (*i*) the difference in Raman shifts of the two $(OH)_a$ and $(OH)_b$ groups bonded to the M2M2M2 triplet of the same type is constant, and (*ii*) the influence of polarizability effect on the spectral position of component bands is proportional to the number of ^{M2}Ca atoms substituted by ^{M2}Mn*. If x is the effect from the first-type influence and y from the second, the width of the spectral range of the O–H stretching mode in Mn-enriched apatites may be written as: $x_{Mn*Mn*Mn*} + (x + y)_{Mn*Mn*Ca} + (x + 2y)_{Mn*CaCa} + (x + 3y)_{CaCaCa} = 3572 - A$, where A [= 3377.5(1) cm^{-1}] denotes the peak position of the $(OH)_a$-Mn*Mn*Mn* triplet obtained from the deconvolution of the pieczkaite Sz29 spectrum,

and 3572 cm^{-1} is the position of the OH stretching mode in hydroxylapatite (Fowler 1974; Tsuda and Arends 1994; Rehman and Bonfield 1997; Zakharov et al. 2004). Although the equation cannot be directly solved, we tested its reliability by deconvoluting the recorded spectra with various x and y values. The best fitting results were obtained for x = 31 cm^{-1} and y = 11.75 cm^{-1}. Finally, all the spectra were deconvoluted into eight position-fixed component bands with the constant predicted centers as presented in Table 2.

APPLICATION TO CRYSTAL CHEMISTRY OF APATITES

The holotype parafiniukite has the empirical formula $(Mn_{2.39}Ca_{2.34}Fe_{0.22}Mg_{0.03}Na_{0.01})_{\Sigma 4.99}P_{3.00}O_{12}[Cl_{0.48}(OH)_{0.41}F_{0.11}]$. Together with the Cross Lake pieczkaite, they are the only Mn-dominant apatites, for which solved crystal structures have been published so far (Tait et al. 2015, Pieczka et al. 2018). Figure 6a shows the representative Raman spectrum of parafiniukite Sz31 in the 3300–3600 cm^{-1} range with the maximum at 3485 cm^{-1}. The spectrum was resolved into seven component bands with predicted Raman shift values and with heights and sometimes also FWHM treated as free parameters (the band at 3409 cm^{-1} zeroed; Table 3). Each of the eight characteristic (OH)-$(M2)_3$ arrangements is characterized by the fitted integral intensity. These data allow the determination of the average composition of M2M2M2 triplet in the parafiniukite Sz31 as $(Mn^*_{1.16}Ca^*_{1.84})_{\Sigma 3}$. Because the X site is occupied by OH + F only in 52 %, the ^{X}(OH + F) site is bonded to 0.60 Mn* + 0.96 Ca apfu (in calculations F was added to OH due to the substitution F→OH rarely observed in Mn-rich apatites; in the studied samples only in Sz31). Taking into account this observation and the M2-site population of 1.94Mn* + 1.06Ca determined by single-crystal X-ray diffraction (Pieczka et al. 2018), we conclude that the averaged M2 triplet bonded to ^{X}Cl must comprise 1.34 Mn* and 0.10 Ca apfu. In consequence, the structural formula of the holotype parafiniukite can be rewritten as

311 $(Ca_{1.29}Mn^*_{0.71})_{\Sigma 2}{}^{M2}(Mn^*_{1.94}Ca_{1.06})_{\Sigma 3}(PO_4)_3(Cl_{0.48}OH_{0.41}F_{0.11})$. This occupancy of the M2M2M2
312 tripled bonded to OH is similar to the occupancy estimated from the O–H band shift in the
313 Raman spectrum. Both suggest a slightly different distribution of Ca in the M2 triplets bonded to
314 ^{X}(OH/F) and ^{X}Cl than was assumed by Tait et al. (2015) for the holotype pieczkaite. However,
315 our results confirm that there is a real preference for ^{M2}Ca to be bonded to ^{X}(OH/F) and ^{M2}Mn* to
316 ^{X}Cl in the apatite structure. The results also indicate that ~90% ^{M2}Ca is bonded to hydroxyl
317 groups, and the remaining ~10% ^{M2}Ca to chlorine anions. It is noteworthy that the averaged
318 ^{X}(OH,F)…M2M2M2 triplet, $(Mn^*_{1.16}Ca_{1.84})_{\Sigma 3}$, calculated from the O–H stretching positions of
319 the component bands, differs slightly from $(Mn^*_{1.36}Ca_{1.64})_{\Sigma 3}$ calculated on the basis of OH band
320 shift. However, the difference can easily be explained by the asymmetric shape of the O–H
321 stretching mode in the mineral.

322 Pieczkaite Sz29 has the empirical composition
323 $(Mn_{4.49}Fe_{0.47}Ca_{0.05}Mg_{0.01})_{\Sigma 5.01}P_{2.99}O_{12}[Cl_{0.83}(OH)_{0.17}]$, close to the end-member formula. Figure 6b
324 shows its Raman spectrum in the range 3300–3600 cm^{-1}, with the peak centered at 3380 cm^{-1}. The
325 spectrum was resolved into seven of the eight predicted component bands (the band at 3409 cm^{-1} also
326 zeroed; Table 3). Similar calculations as for parafiniukite Sz31 give the averaged OH-M2M2M2
327 triplet as $(Mn^*_{2.49}Ca_{0.51})_{\Sigma 3}$ and, with the presence of only 0.17 ^{X}OH apfu, lead to 0.42 Mn* + 0.09 Ca
328 apfu at the M2 sites bonded to the OH group. Therefore, the most probable structural formula of the
329 pieczkaite Sz29 is $^{M1}Mn^*_{2.00}{}^{M2}(Mn^*_{2.95}Ca_{0.05})_{\Sigma 3}(PO_4)_3(Cl_{0.83}OH_{0.17})$, with the presence of all Ca
330 determined by EPMA at the M2 site.

331 Applying the same strategy and assuming the possible presence of Ca at the M2 sites bonded to
332 ^{X}Cl at an amount of ~1/10 of the Ca bonded to ^{X}(OH), the following structural formulas (and
333 resulting classification) may be evaluated for the other crystals studied:

334 **Sz97/2**: $^{M1}(Ca_{1.06}Mn^*_{0.94})_{\Sigma 2}{}^{M2}(Mn^*_{2.54}Ca_{0.47})_{\Sigma 3}(PO_4)_3(Cl_{0.66}OH_{0.34})$ → parafiniukite,

Sz97/6: $^{M1}(Mn^*_{1.47}Ca_{0.53})_{\Sigma 2}{}^{M2}(Mn^*_{2.63}Ca_{0.37})_{\Sigma 3}(PO_4)_3(Cl_{0.73}OH_{0.27})$ → pieczkaite,

Sz108/6: $^{M1}(Ca_{1.19}Mn^*_{0.81})_{\Sigma 2}{}^{M2}(Mn^*_{2.68}Ca_{0.32})_{\Sigma 3}(PO_4)_3(Cl_{0.74}OH_{0.26})$ → parafiniukite,

Sz108/9: $^{M1}(Mn^*_{1.48}Ca_{0.52})_{\Sigma 2}{}^{M2}(Mn^*_{2.71}Ca_{0.29})_{\Sigma 3}(PO_4)_3(Cl_{0.76}OH_{0.24})$ → pieczkaite.

IMPLICATIONS

Detailed analysis of the O–H stretching vibration mode in (Mn,Cl)-rich apatites allows us to evaluate the distribution of Ca- and Mn*-type cations on the M1 and M2 sites in the apatite structure. It also yields direct quantitative information about the content of Mn* at the M2 sites bonded to hydroxyl, and can be used for the verification of the single-crystal-determined M2-site occupancy. Our results show that the assumption that all ^{M2}Ca must be bonded to OH groups (Tait et al. 2015), concluded on the basis of single-crystal X-ray diffraction studies of the holotype pieczkaite, is only partly fulfilled, and in the holotype parafiniukite Sz31 a small portion of ^{M2}Ca (~10 %) is bonded to Cl. This observation should be taken into consideration in future studies of Mn-bearing apatites.

The classification of (Mn,Cl)-rich mineral specimens with compositions corresponding to pieczkaite and parafiniukite almost always requires structural analysis, because the distinction between the two species depends on the Mn-Ca ordering on the M1 and M2 sites. The analysis of the position and fine structure of the O–H stretching band in Raman spectra of (Mn,Cl)-rich apatites has shown that samples with total Mn content close to, or above, 4 apfu, represent pieczkaite, but those with ~3.5 or less Mn apfu most probably represent parafiniukite. This observation requires verification by additional single-crystal X-ray diffraction studies. Similar analysis of the O–H stretching vibration mode in Mn-bearing fluor-hydroxylapatite, not studied in the current research, may be a useful tool in searching for two other hypothetical mineral species of the apatite supergroup, i.e. $Mn_2Ca_3(PO_4)_3F$ and $Mn_2Ca_3(PO_4)_3OH$.

Due to the high spatial resolution of micro-Raman spectroscopy, structural information can be obtained from a very small sample volume, several hundred to several hundreds of thousands times smaller than in the case of single-crystal X-ray diffraction. This offers various possibilities in micro- to nano-scale studies. Together with microtextural analysis, it can be a very useful tool in studying Mn-bearing apatite crystallization processes or high- to low-temperature alteration in late Mn-enriched environments. Moreover, the method can also be easily adjusted to modern apatite-type synthetic nanomaterials with various biomedical and industrial applications.

ACKNOWLEDGEMENTS

We thank two anonymous reviewers for valuable comments on the manuscript. We are also very indebted to Fabrizio Nestola for careful editorial handling. The studies were supported by the National Science Centre (Poland) grant 2015/17/B/ST10/03231 to AP.

REFERENCES

Cuscó, R., Guitian, F., de Aza, S. and Artus, L. (1998) Differentiation between hydroxyapatite and beta-tricalcium phosphate by means of mu-raman spectroscopy. Journal of the European Ceramic Society, 18, 1301–1305.

Fowler, B.O. (1974) Infrared studies of apatites: I. Vibrational assigments for calcium, strontium, and barium hydroxyapatites utilizing isotopic substitution. Inorganic Chemistry, 13, 194–207.

Hughes, J.M., Ertl, A., Bernhardt, H.J., Rossman, G.R. and Rakovan, J. (2004) Mn-rich fluorapatite from Austria: Crystal structure, chemical analysis and spectroscopic investigations. American Mineralogist, 89, 629–632.

Hughes, J.M., Harlov, D., Kelly, S.R., Rakovan, J. and Wilke, M. (2016) Solid-solution in the apatite OH–Cl binary system. Compositional dependence of solid-solution mechanisms in calcium phosphate apatites along the Cl–OH binary. American Mineralogist, 101, 1783–1791.

Levenberg, K. (1944) A method for the solution of certain non-linear problems in least squares. Quarterly of Applied Mathematics, 2, 164–168.

Marquardt, D. (1963) An algorithm for least-squares estimation of nonlinear parameters". SIAM Journal on Applied Mathematics, 11, 431–441

Pasero, M., Kampf, A.R., Ferraris, C., Pekov, I.V., Rakovan, J. and White, T.J. (2010) Nomenclature of the apatite supergroup minerals. European Journal of Mineralogy, 22, 163–179.

Penel, G., Cau, E., Delfosse, C., Rey, C., Hardouin, P., Jeanfils, J., Delecourt, C., Lemaitre, J. and Leroy, G. (2003) Raman microspectrometry studies of calcified tissues and related biomaterials. Dental and Medical Problems, 40, 37–43.

Pieczka, A., Biagioni, C., Gołębiowska, B., Jeleń, P., Pasero, M. and Sitarz, M. (2018) Parafiniukite, $Ca_2Mn_3(PO_4)_3Cl$, a new member of the apatite supergroup from the Szklary pegmatite, Lower Silesia, Poland: Description and crystal structure. Minerals, 8, 485; doi:10.3390/min8110485.

Pouchou, J.-L. and Pichoir, F. (1991) Quantitative analysis of homogeneous or stratified microvolumes applying the model "PAP". In Electron Probe Quantitation; Heinrich, K.F.J., Newbury, D.E., eds., Plenum Press: New York, NY, USA, 1991; pp. 3l–75.

Rehman, I. and Bonfield, W. (1997) Characterization of hydroxyapatiteband carbonated apatite by photo acoustic FTIR spectroscopy. Journal of Materials Science-Materials in Medicine, 8, 1–4.

Suitch, P.R., Lacout, J.L., Hewat, A.W. and Young, R.A. (1985) The structural location and role of Mn^{2+} partially substituted for Ca^{2+} in fluorapatite. Acta Crystallographica, B41, 173–179.

Szuszkiewicz, A., Pieczka, A., Gołębiowska, B., Dumańska-Słowik, M., Marszałek, M., Szełęg, E. (2018) Chemical composition of Mn- and Cl-rich apatites from the Szklary pegmatite, Central Sudetes, SW Poland: Taxonomic and genetic implications. Minerals, 8, 350; doi:10.3390/min8080350.

Tait, K.T., Hawthorne, F.C. and Černý, P. (2011) Minerals from the Cross Lake pegmatite, Manitoba, Canada. 5th International Symposium on Granitic Pegmatites, PEG 2011, Mendoza, Argentina. Conference Papers. Asociación Geologica Argentina, Serie D, Publicación Especial, 14, 213–215.

Tait, K., Ball, N.A. and Hawthorne, F.C. (2015) Pieczkaite, ideally $Mn_5(PO_4)_3Cl$, a new apatite-supergroup mineral from Cross Lake, Manitoba, Canada: Description and crystal structure. American Mineralogist, 100, 1047–1052.

Tsuda, H. and Arends, J. (1994) Orientational micro-Raman spectroscopy on hydroxyapatite single crystals and human enamel crystallites. Journal of Dental Research, 73, 1703–1710.

Twardak, D. and Pieczka, A. (2018) Phosphates in the Julianna pegmatitic system at Piława Górna, Góry Sowie Block. Joint 5th Central-European Mineralogical Conference and 7th Mineral Sciences in the Carpathians Conference, Banská Štiavnica, June 26–30, 2018. Book of Abstracts, 108.

Wojdyr, M. (2010) Fityk, a general-purpose peak fitting program. Journal of Applied Crystallography 43, 1126–1128.

Zakharov, N.A., Polunina, I.A. Polunin, K.E., Rakitina, N.M., Kochetkova, E.I., Sokolova, N.P. and Kalinnikov, V.T. (2004) Calcium hydroxyapatite for medical applications. Inorganic Materials, 40, 641–648.

Figure captions:

Figure 1. Back-scattered electron image of pieczkaite Sz29 relics.

Figure 2. Raman spectra of the (Mn,Cl)-rich apatites in the range 50–4000 cm^{-1}.

Figure 3. O–H stretching vibration region for pieczkaite Sz29.

Figure 4. Deconvolution of O–H stretching vibration band in the spectra of the (Mn,Cl)-rich apatites into four component bands with fixed spectral positions: parafiniukite Sz31 (**a**); pieczkaite Sz29 (**b**); parafiniukite Sz97/2 (**c**); pieczkaite Sz97/6 (**d**), parafiniukite Sz108/6 (**e**); pieczkaite Sz108/9 (**f**). Colors: black – recorded spectrum, green – component bands, red – the spectrum modeled, blue – plot of residuals.

Figure 5. Deconvolution of O–H stretching vibration band in the spectra of the (Mn,Cl)-rich apatites into four bands with fixed border and two free intermediate bands. Sample labels and colors as in Figure 4.

Figure 6. Deconvolution of O–H stretching vibration band in the spectra of the (Mn,Cl)-rich apatites into eight predicted bands (compare Table 2). Sample labels and colors as in Figure 4.

This is a preprint, the final version is subject to change, of the American Mineralogist (MSA)
Cite as Authors (Year) Title. American Mineralogist, in press.
DOI: https://doi.org/10.2138/am-2020-7324

Table 1. Chemical composition of the studied (Mn,Cl)-rich apatites.

Constituent	Sz29 *n=5*	Sz31* *n=16*	Sz97/2 *n=4*	Sz97/6 *n = 9*	Sz108/6 *n=6*	Sz108/9 *n=8*
P_2O_5 (wt%)	36.65(45)	39.20(14)	37.21(41)	36.88(29)	38.04(33)	36.99(74)
FeO	5.63(30)	2.95(16)	2.21(39)	3.85(70)	3.29(88)	5.28(94)
MnO	53.46(56)	31.19(62)	41.22(36)	46.38(1.2)	40.61(2.0)	45.92(46)
MgO	0.07(02)	0.19(05)	0.04(02)	0.10(04)	0.08(04)	0.16(3)
CaO	0.42(17)	24.14(39)	14.84(69)	8.45(1.5)	14.95(2.3)	7.71(82)
SrO	0.01(04)	b.d.l.	0.24(19)	0.04(09)	0.42(26)	0.29(26)
Na_2O	b.d.l.	0.05(02)	0.16(03)	0.18(05)	b.d.l.	b.d.l.
F	b.d.l.	0.39(05)	b.d.l.	b.d.l.	b.d.l.	b.d.l.
Cl	4.96(21)	3.13(09)	4.12(03)	4.50(31)	4.68(17)	4.67(5)
$H_2O_{(calc)}$	0.25(05)	0.68(03)	0.53(01)	0.42(08)	0.42(04)	0.38(3)
O = (F + Cl)	-1.12(05)	-0.87(04)	0.93(01)	-1.02(07)	-1.06(04)	-1.05(1)
Total	99.34	101.04	99.64	99.79	101.43	100.36
apfu						
P^{5+}	2.99(2)	3.00(1)	2.99(1)	3.00(1)	3.00(1)	3.00(2)
Fe^{2+}	0.47(3)	0.22(1)	0.18(3)	0.31(6)	0.26(7)	0.42(8)
Mn^{2+}	4.49(4)	2.39(4)	3.31(5)	3.78(9)	3.21(17)	3.73(5)
Mg^{2+}	0.01(0)	0.03(1)	0.01(0)	0.02(1)	0.01(1)	0.02(0)
Ca^{2+}	0.05(2)	2.34(4)	1.51(6)	0.87(15)	1.49(22)	0.79(8)
Sr^{2+}	0.00(0)	0	0.01(1)	0.00(1)	0.02(1)	0.02(10
Na^{+}	0	0.01(0)	0.03(1)	0.03(1)	0	0
F^{-}	0	0.11(1)	0	0	0	0
Cl^{-}	0.83(3)	0.48(1)	0.66(1)	0.73(5)	0.74(3)	0.76(1)
OH^{-}	0.17(3)	0.41(2)	0.34(1)	0.27(5)	0.26(3)	0.24(1)
Σcations	5.01(4)	4.99(2)	5.04(3)	5.01(3)	4.99(2)	4.99(5)

Notes: *n* – number of spot analyses; numbers in parentheses – estimated standard deviations, b.d.l. – below detection limit, * – parafiniukite analysis from Pieczka et al. (2018).

This is a preprint, the final version is subject to change, of the American Mineralogist (MSA)
Cite as Authors (Year) Title. American Mineralogist, in press.
DOI: https://doi.org/10.2138/am-2020-7324

Table 2. Possible OH…$(M2)_3$ arrangements and the predicted Raman shifts (cm^{-1}).

OH…$(M2)_3$ arrangement	Predicted Raman shift (cm^{-1})
$(OH)_a$-Mn*Mn*Mn*	3377.5
$(OH)_b$-Mn*Mn*Mn*	3409
$(OH)_a$-Mn*Mn*Ca	3420
$(OH)_b$-Mn*Mn*Ca	3451
$(OH)_a$-Mn*CaCa	3475
$(OH)_b$-Mn*CaCa	3506
$(OH)_a$-CaCaCa	3541
$(OH)_b$-CaCaCa	3572

Mn* = Mn + Fe + Mg.

This is a preprint, the final version is subject to change, of the American Mineralogist (MSA)
Cite as Authors (Year) Title. American Mineralogist, in press.
DOI: https://doi.org/10.2138/am-2020-7324

Table 3. Deconvolution of the O–H stretching band and its crystal chemical interpretation.

Sample R^2	Raman shift (cm^{-1})	FWHM (cm^{-1})	Integral intensity (%)	$OH\ldots(M2)_3$ arrangement	Mn* (*apfu*)	Ca (*apfu*)
29	3377.5(1)	47.4(3)	71.16	$(OH)_a$–Mn*Mn*Mn*	2.13	0.00
0.986	3409	-	0.00	$(OH)_b$–Mn*Mn*Mn*	0.00	0.00
	3420	29	9.81	$(OH)_a$–Mn*Mn*Ca	0.20	0.10
	3451	25(2)	5.09	$(OH)_b$–Mn*Mn*Ca	0.10	0.05
	3475	24	2.55	$(OH)_a$–Mn*CaCa	0.03	0.05
	3506	30	3.40	$(OH)_b$–Mn*CaCa	0.03	0.07
	3541	38(4)	4.43	$(OH)_a$–CaCaCa	0.00	0.13
	3572	40	3.55	$(OH)_b$–CaCaCa	0.00	0.11
			100.0	*Total*	2.49	0.51
				OH = 0.17 *apfu*	0.42	0.09
31	3377.5	36(3)	2.58	$(OH)_a$–Mn*Mn*Mn*	0.08	0.00
0.988	3409	-	0.00	$(OH)_b$–Mn*Mn*Mn*	0.00	0.00
	3420	43(2)	9.50	$(OH)_a$–Mn*Mn*Ca	0.19	0.10
	3451	50	12.35	$(OH)_b$–Mn*Mn*Ca	0.25	0.12
	3475	50	41.97	$(OH)_a$–Mn*CaCa	0.42	0.84
	3506	39(1)	22.48	$(OH)_b$–Mn*CaCa	0.22	0.45
	3541	26(2)	4.46	$(OH)_a$–CaCaCa	0.00	0.13
	3572	43(3)	6.66	$(OH)_b$–CaCaCa	0.00	0.20
			100.0	*Total*	1.16	1.84
				OH + F = 0.52 *apfu*	0.60	0.96
97/2	3377.5	31(2)	2.42	$(OH)_a$–Mn*Mn*Mn*	0.07	0.00
0.997	3409	35(2)	5.42	$(OH)_b$–Mn*Mn*Mn*	0.16	0.00
	3420	17(2)	1.01	$(OH)_a$–Mn*Mn*Ca	0.02	0.01
	3451	67(1)	68.98	$(OH)_b$–Mn*Mn*Ca	1.38	0.69
	3475	36	4.46	$(OH)_a$–Mn*CaCa	0.04	0.09
	3506	39(1)	9.32	$(OH)_b$–Mn*CaCa	0.09	0.19
	3541	26(1)	2.85	$(OH)_a$–CaCaCa	0.00	0.09
	3572	44	5.54	$(OH)_b$–CaCaCa	0.00	0.17
			100.00	*Total*	1.77	1.23
				OH = 0.34 *apfu*	0.60	0.42
97/6	3377.5	33(1)	6.15	$(OH)_a$–Mn*Mn*Mn*	0.18	0.00
0.999	3409	38	4.06	$(OH)_b$–Mn*Mn*Mn*	0.12	0.00
	3420	45(1)	51.20	$(OH)_a$–Mn*Mn*Ca	1.02	0.51
	3451	32(1)	14.53	$(OH)_b$–Mn*Mn*Ca	0.29	0.15
	3475	36(1)	11.74	$(OH)_a$–Mn*CaCa	0.12	0.23
	3506	39(2)	5.23	$(OH)_b$–Mn*CaCa	0.05	0.10
	3541	35(2)	2.29	$(OH)_a$–CaCaCa	0.00	0.07
	3572	50	4.79	$(OH)_b$–CaCaCa	0.00	0.14
			100.00	*Total*	1.79	1.21
				OH = 0.27 *apfu*	0.48	0.33
108/6	3377.5	42(3)	4.37	$(OH)_a$–Mn*Mn*Mn*	0.13	0.00
0.992	3409	28(1)	8.72	$(OH)_b$–Mn*Mn*Mn*	0.26	0.00
	3420	16(3)	1.21	$(OH)_a$–Mn*Mn*Ca	0.02	0.01
	3451	49(1)	64.11	$(OH)_b$–Mn*Mn*Ca	1.28	0.64
	3475	28	6.81	$(OH)_a$–Mn*CaCa	0.07	0.14
	3506	33(1)	11.23	$(OH)_b$–Mn*CaCa	0.11	0.22
	3541	25(3)	1.94	$(OH)_a$–CaCaCa	0.00	0.06
	3572	28(4)	1.61	$(OH)_b$–CaCaCa	0.00	0.05
			100.00	*Total*	1.88	1.12
				OH = 0.26 *apfu*	0.49	0.29
108/9	3377.5	40	5.03	$(OH)_a$–Mn*Mn*Mn*	0.15	0.00
0.992	3409	23(6)	0.92	$(OH)_b$–Mn*Mn*Mn*	0.03	0.00
	3420	45(1)	32.55	$(OH)_a$–Mn*Mn*Ca	0.65	0.33
	3451	50	51.15	$(OH)_b$–Mn*Mn*Ca	1.02	0.51
	3475	-	0.00	$(OH)_a$–Mn*CaCa	0.00	0.00

This is a preprint, the final version is subject to change, of the American Mineralogist (MSA)
Cite as Authors (Year) Title. American Mineralogist, in press.
DOI: https://doi.org/10.2138/am-2020-7324

3506	43(2)	7.99	$(OH)_b$–Mn*CaCa	0.08	0.16
3541	-	0.00	$(OH)_a$–CaCaCa	0.00	0.00
3572	45(6)	2.36	$(OH)_b$–CaCaCa	0.00	0.07
		100.00	*Total*	1.93	1.07
			OH = 0.24 *apfu*	0.46	0.26

Notes: FWHM – full-width at half maximum, Mn* = Mn + Fe + Mg. Numbers in parentheses denote standard deviations. The FWHMs without standard deviations are fixed.

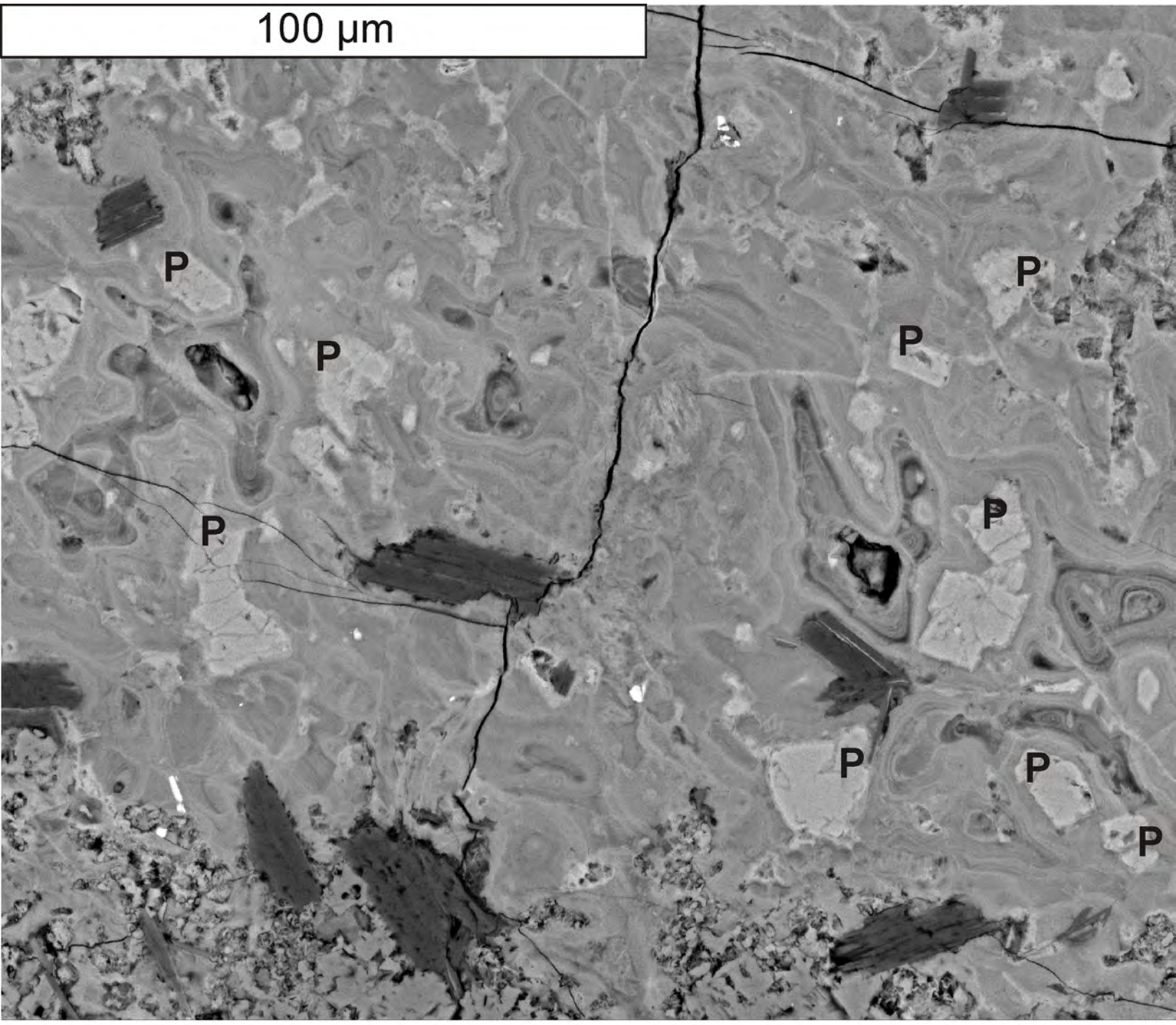

Fig. 1.

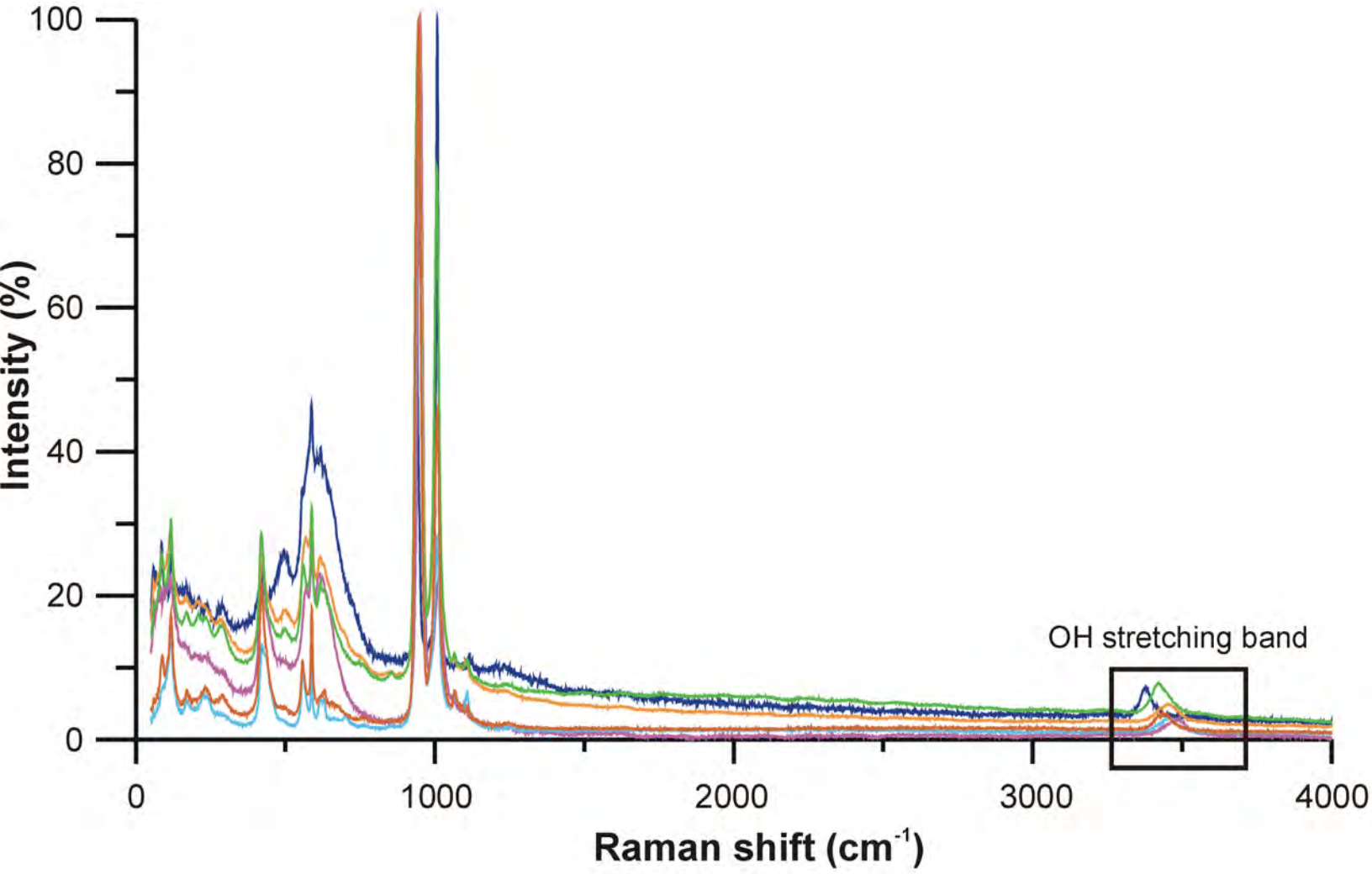
100
80
60
40
20
0
Intensity (%)
OH stretching band
0
1000
2000
3000
4000
Raman shift (cm-1)

Fig. 2.

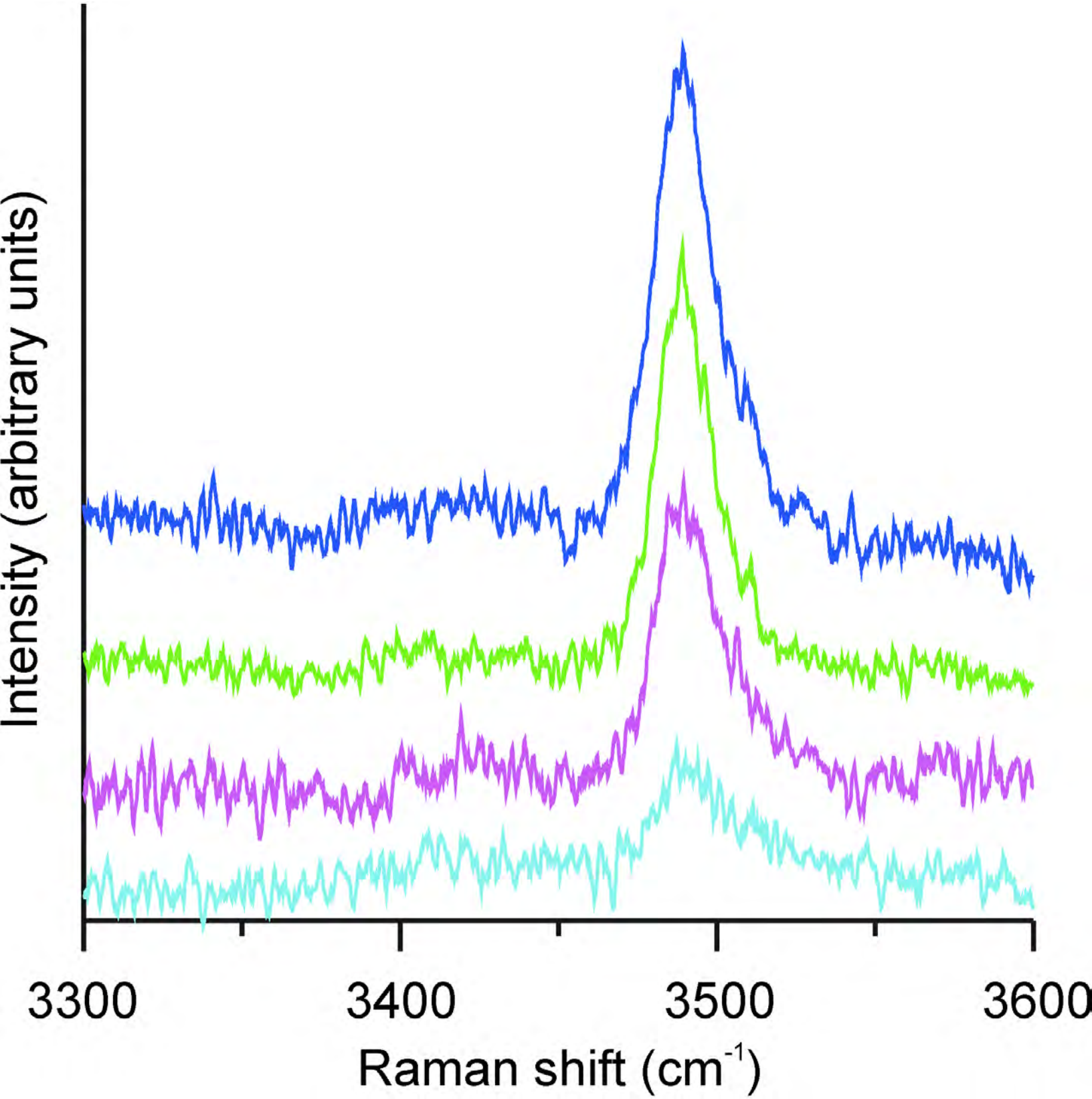
Intensity (arbitrary units)
3300
3400
3500
3600
Raman shift (cm-1)

Fig. 3.

Fig. 4

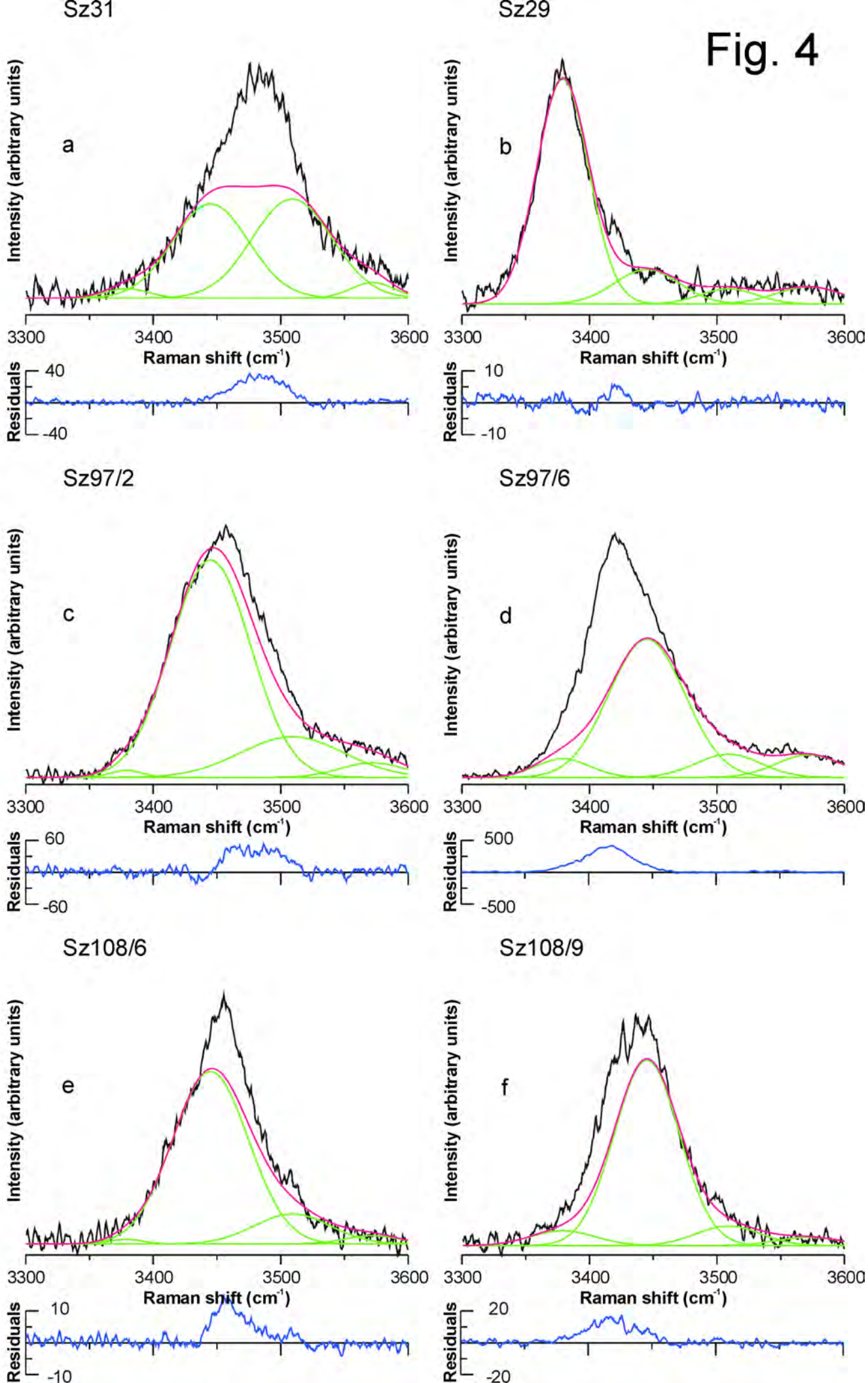
Sz31
Sz29
a
b
Intensity (arbitrary units)
3300
3400
3500
3600
Raman shift (cm-1)
Residuals
40
-40
10
-10
Sz97/2
Sz97/6
c
d
60
-60
500
-500
Sz108/6
Sz108/9
e
f
20
-20

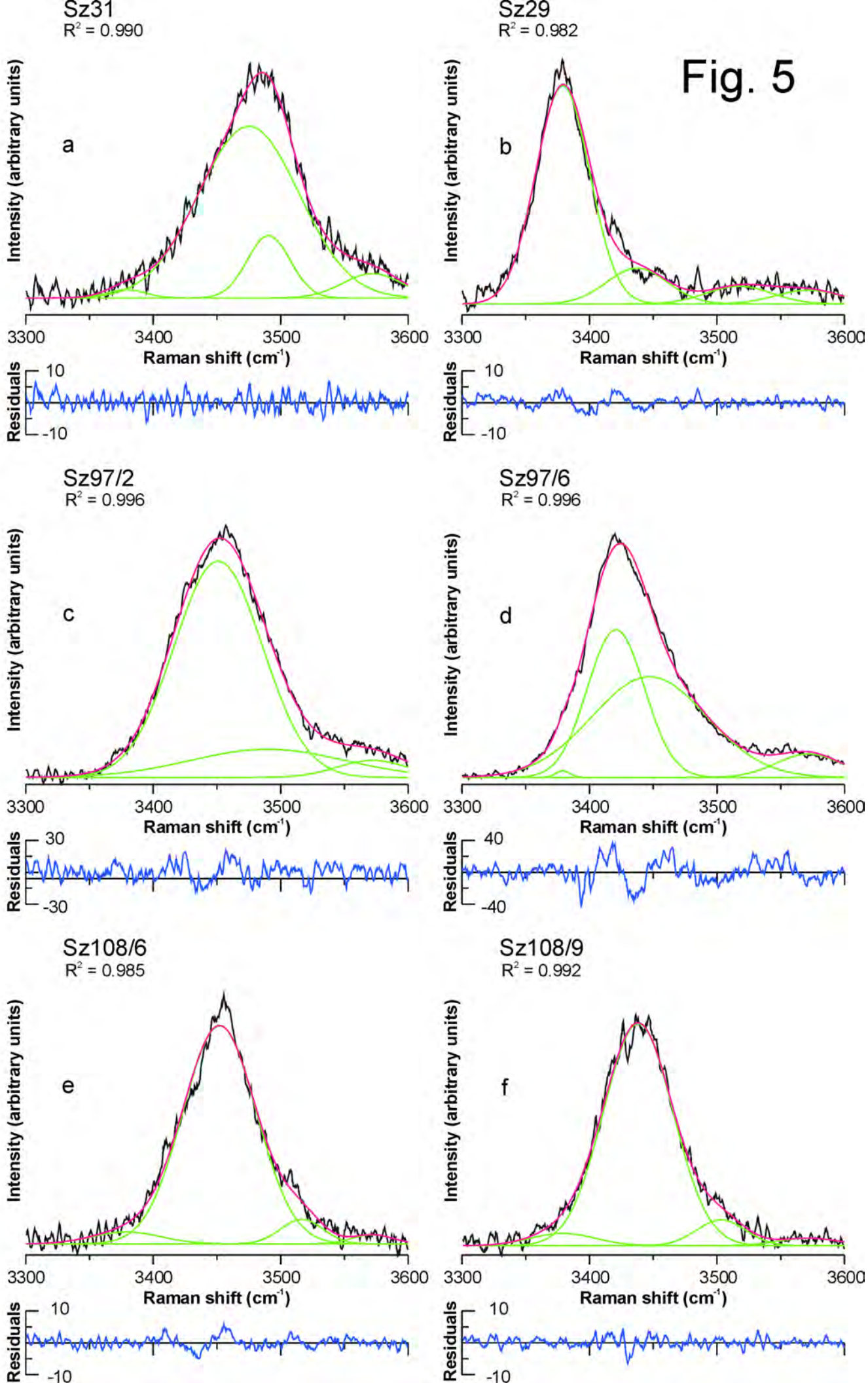
Sz31
R² = 0.990
Sz29
R² = 0.982
Fig. 5
a
b
Intensity (arbitrary units)
Raman shift (cm⁻¹)
Residuals
10
-10
Sz97/2
R² = 0.996
Sz97/6
R² = 0.996
c
d
30
-30
40
-40
Sz108/6
R² = 0.985
Sz108/9
R² = 0.992
e
f
3300
3400
3500
3600

Fig. 6

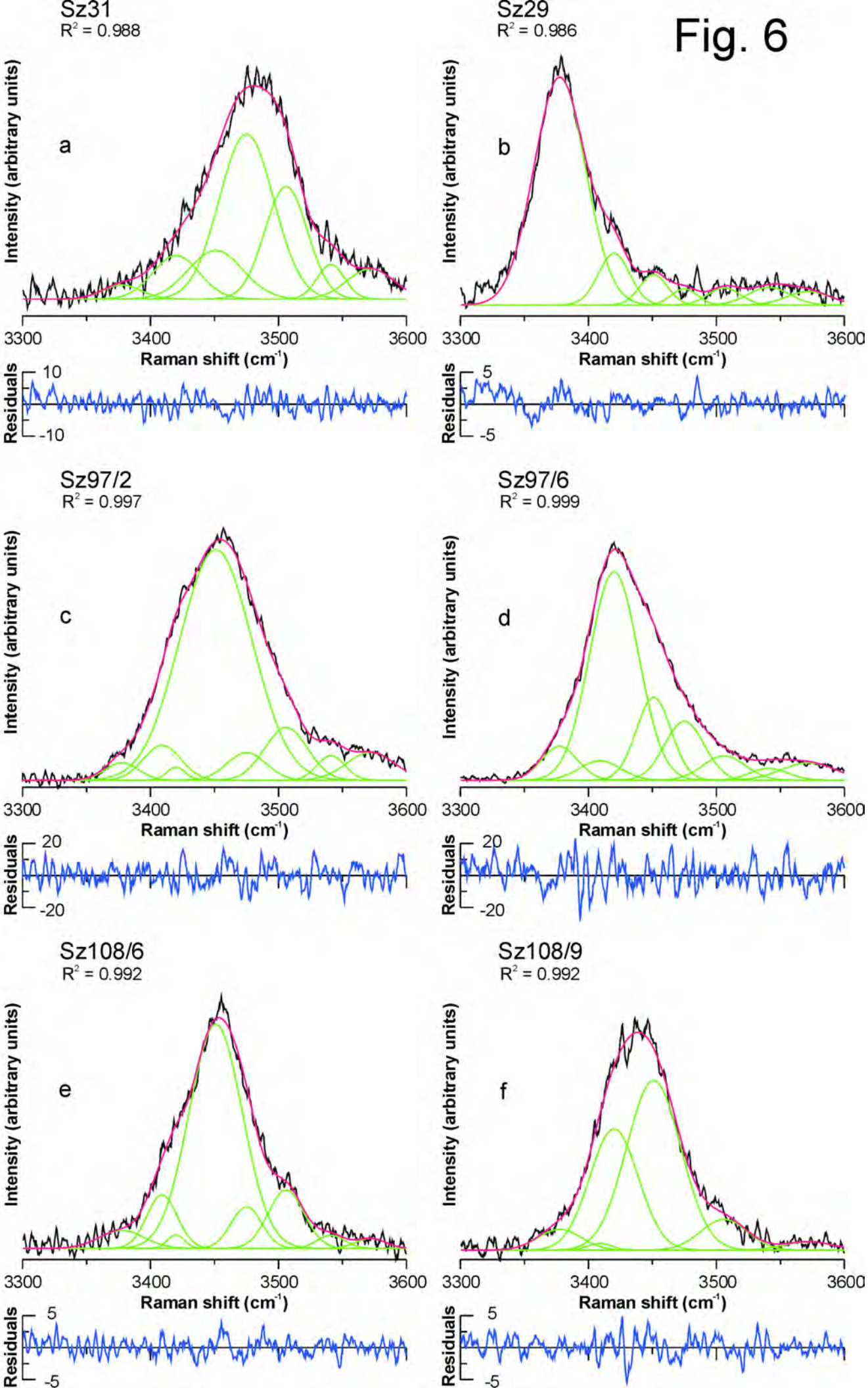
Sz31
R² = 0.988
a
Intensity (arbitrary units)
3300
3400
3500
3600
Raman shift (cm⁻¹)
Residuals
10
-10
Sz29
R² = 0.986
b
Intensity (arbitrary units)
3300
3400
3500
3600
Raman shift (cm⁻¹)
Residuals
5
-5
Sz97/2
R² = 0.997
c
Intensity (arbitrary units)
3300
3400
3500
3600
Raman shift (cm⁻¹)
Residuals
20
-20
Sz97/6
R² = 0.999
d
Intensity (arbitrary units)
3300
3400
3500
3600
Raman shift (cm⁻¹)
Residuals
20
-20
Sz108/6
R² = 0.992
e
Intensity (arbitrary units)
3300
3400
3500
3600
Raman shift (cm⁻¹)
Residuals
5
-5
Sz108/9
R² = 0.992
f
Intensity (arbitrary units)
3300
3400
3500
3600
Raman shift (cm⁻¹)
Residuals
5
-5